GA–A25857

INTEGRATED SCENARIO MODELING OF DIII-D AT DISCHARGES UTILIZING FAST WAVE HEATING AND CURRENT DRIVE

by

J.M. PARK, M. MURAKAMI, H.E. ST JOHN, L.L. LAO, J.R. FERRON, and R. PRATER

JULY 2007

GENERAL ATOMICS

DISCLAIMER

GA–A25857

INTEGRATED SCENARIO MODELING OF DIII-D AT DISCHARGES UTILIZING FAST WAVE HEATING AND CURRENT DRIVE

by
J.M. PARK,* M. MURAKAMI,* H.E. ST JOHN, L.L. LAO, J.R. FERRON, and R. PRATER

This is a preprint of a paper to be presented at the 34th EPS Conf. on Plasma Physics, in Warsaw, Poland, July 2-7, 2007 and to be published in the *Proceedings.*

*Oak Ridge National Laboratory, Oak Ridge, Tennessee.

Work supported by
the U.S. Department of Energy
under DE-AC05-00OR22725 and DE-FC02-04ER54698

GENERAL ATOMICS PROJECT 30200
JULY 2007

GENERAL ATOMICS

Integrated Scenario Modeling of DIII-D AT Discharges Utilizing Fast Wave Heating and Current Drive

J.M. Park,[1] M. Murakami,[1] H.E. St John,[2] L.L. Lao,[2] J.R. Ferron,[2] and R. Prater[2]

[1]*Oak Ridge National Laboratory, Oak Ridge, Tennessee 37830, USA*
[2]*General Atomics, P.O. Box 85608, San Diego, California 92186-5608, USA*

I. Introduction

The DIII-D Advanced Tokamak (AT) program is aimed at developing the scientific basis for steady-state and high-performance operation of fusion reactors. Recent experiments with weakly negative central magnetic shear (NCS) achieved performance necessary for ITER Q = 5 steady-state scenarios with normalized fusion performance $G = \beta_N H/q^2 \geq 0.3$ and noninductive fraction $f_{NI} \approx 100\%$ [1]. Present simulations focus on optimizing fully noninductive operation at higher beta by utilizing the fast wave heating and current drive system.

II. Integrated Scenario Modeling with Fast Wave Heating and Current Drive

Integrated scenario modeling has been carried out to guide the AT experiment with the upgraded DIII-D hardware: higher power and longer pulse of fast wave (FW) and electron cyclotron current drive (ECCD), and co- and counter-neutral beam (NB) injection in both a pumped single-null and a double-null divertor configuration. In this predictive modeling, the theory-based, gyro-Landau fluid (GLF23) model is employed with a self-consistent source and sink calculation based on the ONETWO transport code [2]. The GLF23 model uses drift-wave eigenmodes to compute the quasilinear energy, toroidal momentum, and particle fluxes due to ion/electron temperature gradient (ITG/ETG) and trapped electron modes (TEM) [3]. Solving the highly nonlinear, stiff transport model is facilitated by a powerful numerical algorithm: globally convergent Newton method (GCNM), based on modified Newton, trust region, and steepest descent method. The computational efficiency has been improved by a recent parallelization of ONETWO using the domain decomposition method. Although the density equation can be solved with the GLF23 model, most of the simulations discussed here use the density profile from experiments. The source model used for FW power deposition and current drive is the CURRAY ray-tracing code including beam ion damping of the FW power. Neutral beam ions are modeled by the Monte-Carlo code NUBEAM in the new co- and counter-beamline configuration in DIII-D. ECCD is calculated by the TORAY-GA ray-tracing code. The predictive simulation adopts the same β feedback control algorithm as used in DIII-D experiments [4] along with the suggested model for q_0 feedback, where the plasma

control system adjusts the NB and FW powers in an attempt to keep the β waveform and q_0 - q_{min}, respectively.

III. Simulation Results

Predictive simulation was carried out based on the existing target discharges in high bootstrap AT regimes of DIII-D [1]. In this AT scenario, the desired target q profile is prepared by triggering an L-H transition early in the current ramp, which slows the current penetration, resulting in a broad current profile. During the next 2-3 s, β is slowly increased under feedback control, resulting in a highly reproducible target q profile with $q_{min} \approx 2$. The neutral beam power is then increased to raise β_N and maintain it at a programmed value and off-axis ECCD is applied to arrest penetration of the current profile that would result in significant inductive current peaked near the magnetic axis. The ONETWO/GLF23 transport model was benchmarked extensively against these AT discharges by reproducing successfully the experimental electron and ion temperatures, toroidal rotation, and recently the density profiles. The present simulation adds the FW power (P_{FW}) on top of the NB and ECCD powers during high performance phase to optimize fully noninductive operation at higher β.

A large set of predictive transport simulations in the stationary state with fully penetrated current profile is obtained by time-stepping the calculation of all the transport equations for over 5 τ_E (~τ_R) followed by one step steady state solution of the current profile [5]. The P_{FW} scan in Fig. 1 shows that 2 MW of FW power increases the noninductive fraction (f_{NI}) to 100% with a reduced average NB power (P_{NB}) at β_N = 3.8, where the NB power is modulated in the same way as in the DIII-D experiment to keep β_N at a constant value. The FW heating is very efficient at increasing the stored energy of AT plasmas since the heating power is deposited in the localized central region, where most of turbulent ion transport (χ_i) is suppressed by *ExB* shear stabilization and turbulent electron transport (χ_e) is lowest. The efficient FW heating increases β_e as shown in Fig. 2(a) and also improves off-axis ECCD efficiency. The

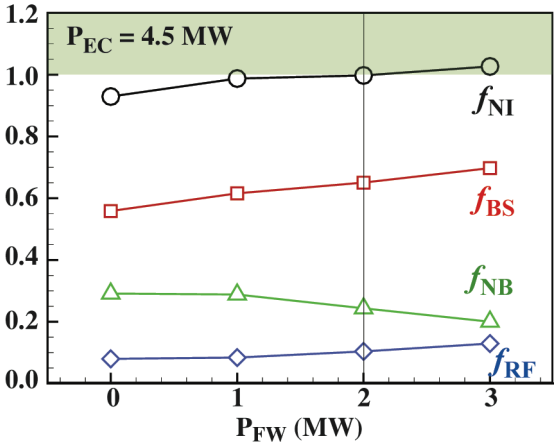

Fig. 1. Noninductive current fraction (circle), and its components: bootstrap current (square), neutral beam current drive (triangle) and fast wave and electron cyclotron current drive (diamond) as a function of fast wave heating power.

bootstrap current increases with P_{FW} due to increased β_e, helping to achieve fully noninductive operation at high β. Higher bootstrap current leads to lower NB power demand in the high performance phase, resulting in better current drive alignment by avoiding excessive central current drive. Figure 2(b) shows the dependency of the noninductive current fraction as a function of β_N for two different values of P_{FW} (P_{FW} = 0 MW and P_{FW} = 2.7 MW) in the ONETWO/GLF23 simulation database. The noninductive fraction increases strongly with β_N for a given P_{FW}, which represents well the experimentally observed trend. These data indicate that the FW heating allows operation at higher f_{NI} with a given β_N.

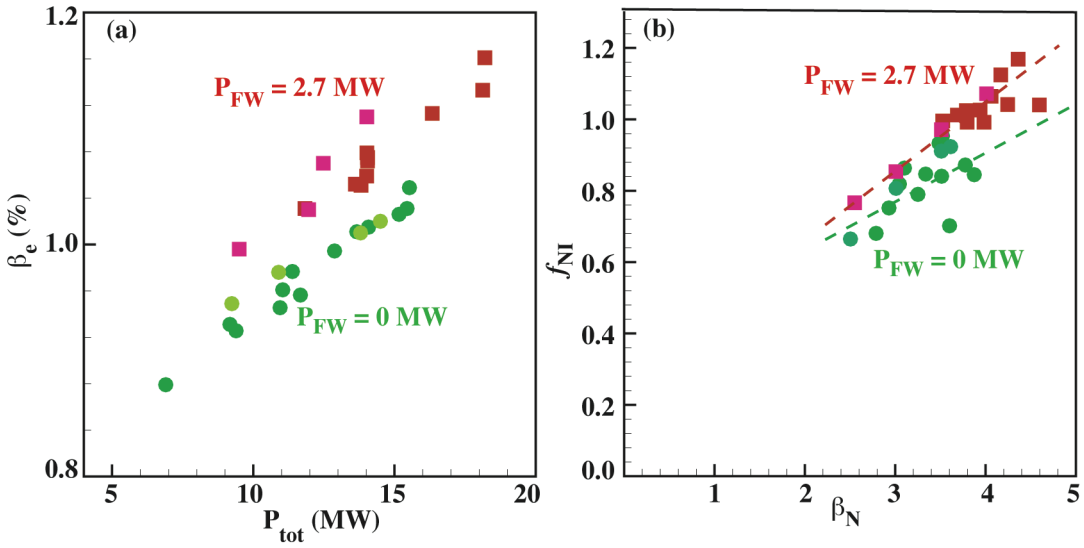

Fig. 2. (a) Electron beta and (b) noninductive current fraction as a function of (a) total heating power and (b) normalized beta for two different fast wave heating power, P_{FW} = 0 MW (circles) and P_{FW} = 2.7 MW (squares), in the ONETWO/GLF23 simulation database.

One of the caveats in this predictive simulation with FW heating and current drive is an uncertainty in estimation of the FW damping on beam ions and its partition to thermal electron and ions. Despite recent advances in theoretical models for beam ion damping of FW, different models disagree [6]. It should also be noted that all prescribed FW power is assumed to be absorbed in the core. However, the edge losses could be important for the weak single pass absorption as in the present cases [6]. Table 1 summarizes the calculated parameters with and without beam ion damping of FW in CURRAY calculation. Although the beam ion damping of FW reduces the fraction of FWCD (f_{FW}) significantly, it is compensated by the increased bootstrap current. Both conservative and optimistic assumptions of FWCD lead to operation at higher β with f_{NI} = 100%.

Table 1: Fully Noninductive High Performance Condition Obtained With and Without Assumption on Beam Ion (BI) Damping of FW

	f_{NI}	f_{BS}	f_{FW}	f_{EC}	β_N	H_{89}	H_{98y2}	G
P_{FW} = 2.7 MW without BI damp	1.01	0.63	0.10	0.07	3.69	2.6	2.1	0.35
P_{FW} = 2.7 MW with BI damp	1.02	0.67	0.05	0.07	3.79	2.7	2.2	0.37

The FWCD is expected to offer a better control of q_0 by active feedback. Figure 3 shows the calculated q_0 with a suggested model feedback control algorithm, where one of two FW launchers at 90 MHz is operated for co- and the other for counter-current drive mode, respectively and the relative current drive power of co- and counter direction is adjusted to keep q_0 and/or q_0 - q_{min} to the programmed value. Figure 3 indicates that 2 MW of P_{FW} allows a fully noninductive operation with a model feedback control q_0 - q_{min} < 0.5.

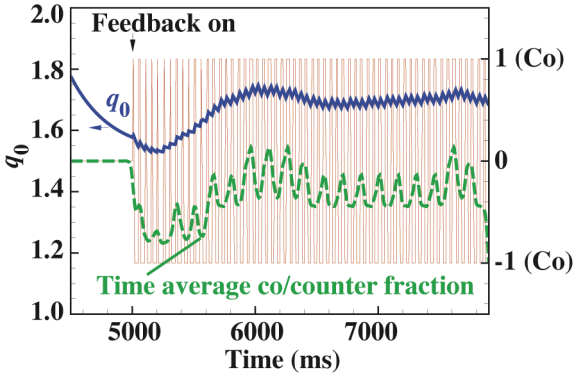

Fig. 3. Calculated time trace of central q with a model feedback control (solid) and relative fraction of co (+1) and counter (-1) current drive (dotted).

IV. Conclusion

GLF23/ONETWO modeling based on the existing target discharge in the high bootstrap AT regime shows that ~2 MW FWCD and 4.5 MW off-axis ECCD leads to fully noninductive operation with bootstrap fraction >60% and normalized fusion performance $G > 0.3$ (ITER $Q = 5$ steady state scenario goal). A database consisting of a large set of predictive transport simulations indicates that fast wave operation offers central heating to improve off-axis ECCD efficiency and an increase in bootstrap current fraction as well as better control of q-profile near the axis. It is demonstrated that modulating input power and co- and counter direction of FWCD allows sustaining favorable q profiles with controlled q_0 - q_{min} < 0.5.

This work was supported by the U.S. Department of Energy under DE-AC05-00OR22725 and DE-FC02-04ER54698.

References

[1] M. Murakami, *et al.*, Phys. Plasmas **13**, 056106 (2006).
[2] H.E. St John, *et al.*, Proc. of the 15th Int. Conf. on Plasma Phys. and Controlled Fusion Research, Seville, Spain (1995).
[3] R.E. Waltz, *et al.*, Phys. Plasmas **4**, 2482 (1997).
[4] J.R. Ferron, *et al.*, Nucl. Fusion **45**, L13 (2006).
[5] H.E. St John, *et al.*, Bull. Am. Phys. Soc. **47**, 302 (2002).
[6] R.I. Pinsker, *et al.*, Proc. 16th Top. Conf. on Radio Frequency Power in Plasmas, Park City, Utah (2005).